

The influence of surface stress on the equilibrium shape of strained quantum dots

N. Moll* and M. Scheffler

Fritz-Haber-Institut der Max-Planck-Gesellschaft, Faradayweg 4-6, D-14195 Berlin-Dahlem, Germany

E. Pehlke

Physik-Department T30, Technische Universität München, D-85747 Garching, Germany

(February 5, 2020)

The equilibrium shapes of InAs quantum dots (*i.e.*, dislocation-free, strained islands with sizes $\geq 10,000$ atoms) grown on a GaAs (001) substrate are studied using a hybrid approach which combines density functional theory (DFT) calculations of microscopic parameters, surface energies, and surface stresses with elasticity theory for the long-range strain fields and strain relaxations. In particular we report DFT calculations of the surface stresses and analyze the influence of the strain on the surface energies of the various facets of the quantum dot. The surface stresses have been neglected in previous studies. Furthermore, the influence of edge energies on the island shapes is briefly discussed. From the knowledge of the equilibrium shape of these islands, we address the question whether experimentally observed quantum dots correspond to thermal equilibrium structures or if they are a result of the growth kinetics.

I. INTRODUCTION

In recent years, the study of growth conditions and electronic properties of quantum dots has attracted significant attention in basic science and technology.^{1–7} Quantum dots are small three-dimensional islands of a low-band-gap semiconductor (e.g. $\text{In}_x\text{Ga}_{1-x}\text{As}$) which are enclosed in a wide-band-gap semiconductor matrix (e.g. GaAs). Provided the bands of these islands and of the host are appropriately aligned, the valence and conduction bands produce a confinement potential for the holes in the valence band and the electrons in the conduction band. If these islands are small enough, they will behave like big artificial atoms with discrete energy levels. Thus, the recombination spectrum of a single quantum dot consists of a single sharp line with a practically not measurable temperature broadening. Quantum dots may be used for new types of devices, as for example a single-electron transistor or cellular automata. Further examples are semiconductor lasers, where the wave length of the emitted light is determined by alloy composition and the size and shape of the dots. Indeed, such lasers have been build in the laboratory.^{5,6} The required size of the quantum dot is dictated by the condition that the energy separation of the quantized electronic levels of the dots should be about 0.1–0.2 eV, so that they are not populated at room temperature. And the dot has to be sufficiently large that at least one bound level exists; for too small islands this is not the case.⁸ For GaInAs these conditions imply that the width of the island is between 50 and 200 Å (or 20–80 atoms), which means that we are dealing with objects built of 1,000–60,000 atoms. For lasers it is necessary to have many dots ($\sim 10^{11}\text{cm}^{-2}$) and these should all have nearly the same size and shape,

so that all dots emit light at practically the same wave length; in a quantum dot laser the width of the line is determined by the size and shape fluctuations of the ensemble of quantum dots which implies that the size and shape uniformity of quantum dots is critical to these applications.

Already in 1990 it had been observed that dislocation-free, strained islands form by itself when InAs is deposited on GaAs,¹ and since 1994 several groups^{2–4} have shown that a range of growth parameters exists at which quantum dots assemble themselves with the desired and tunable size and a rather narrow size distribution. The mechanism giving rise to this self-assembly of the dots is still not understood.

Often the formation of quantum dots is explained in terms of a thermal-equilibrium picture where the system assumes the state of lowest free energy: Islands form, instead of a strained, epitaxial film, because the gain of elastic relaxation energy (possible in an island) overcompensates the cost due to the increased surface energy (a three-dimensional island has a larger surface than a two-dimensional film). Typically such island do not form immediately on the substrate but on top of a wetting layer (see for example Ref. 8). For InAs quantum dots on GaAs (001) this wetting layer has a thickness of about 1.5 monolayers. When this thermal equilibrium picture applies the growth mode giving rise to islands is called the Stranski-Krastanov growth mode.⁹

Other authors have emphasized the role of kinetic effects.^{10–12} Dobbs *et al.*¹² studied the formation of islands using self-consistent rate equations. Their rate theory is designed to predict reliably average quantities and they found that their island density in dependence of the coverage is in good agreement with experiment. But they

could not calculate the island size distribution explicitly.

Because in several experimental as well as theoretical papers^{7,13,14} it is assumed that thermal-equilibrium theory is applicable to describe and understand the formation of quantum dots, we performed calculations of the equilibrium structure to find out whether or not this agrees with results of growth experiments. The calculations are done for dislocation-free InAs islands epitaxially grown on GaAs (001). Knowing the equilibrium shapes is indeed important, because under certain conditions thermal equilibrium will be reached. And in general, if the quantum-dot shape observed in experiments deviates from the equilibrium shape, one has to conclude that equilibrium thermodynamics is not adequate to describe the island formation and the assumed shape and size distribution. We note in passing that the growth of experimental quantum dots is likely affected also by (unwanted) alloying of the dot and the matrix,¹⁵ by entropy effects, and for high concentrations of quantum dots also the island-island interaction has to be considered. These effects are neglected in the present calculations.

The InAs quantum dots of interest contain more than 1,000 atoms. We consider it unwise to evaluate the total energy of such a system by a *direct* density functional calculation. Therefore a hybrid method was developed that provides the same result as a direct approach, but at much less computational costs. Even more importantly, this method exhibits with greater clarity the underlying physical mechanisms. In brief, the approach is summarized as follows. The total energy of a large, isolated quantum dot is given by

$$E^{q\text{-dot}} = E^{\text{elastic}} + E^{\text{surface}} + E^{\text{edge}} . \quad (1)$$

The leading terms are the elastic relaxation energy and the sum over the surface energies of the surface facets. Both quantities depend sensitively on the quantum-dot shape. The surface reconstructions, the surface energies and their strain dependence are calculated by DFT and analyzed as a function of the atomic chemical potential. If the size of an island is bigger than about 1,000 atoms it turns out that the strain fields and elastic energies are well described by elasticity theory because they follow the scaling laws.¹⁶ We therefore evaluate the long-range strain relaxation in the quantum dot and in the underlying substrate by elasticity theory applying a finite-element approach. The approach permits the systematic investigation of almost any island shape. Fig. 1 displays the importance of the different energy contributions and their scaling with island size. These results refer to an isolated, pyramidal shaped quantum dot, but essentially the same behavior is found for other island shapes. The elastic energy of a relaxed quantum dot, compared to the energy of a two-dimensional epitaxial film scales linearly with the volume (or the number of atoms) of the quantum dot. This analytical scaling holds true for the elastic energy as long as the islands contain more than 1,000 atoms. The single facets of the island have to be

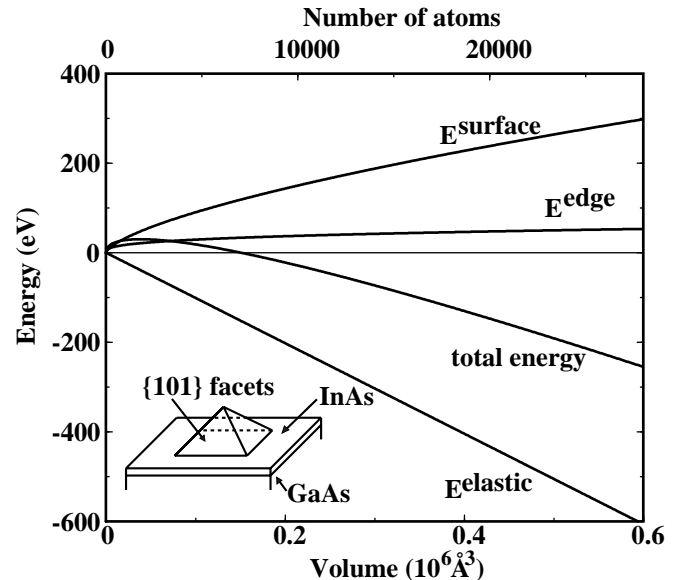


FIG. 1. Energy contributions of a single, pyramidal shaped, dislocation free island compared to the energies of an epitaxial (strained) film. The elastic energy relief E^{elastic} due to the partial strain relaxation, the surface-energy contribution E^{surface} due to the increased surface area, and the contribution due to the various edges E^{edge} are shown. The total energy displays the sum of all these contributions. The applied approach (see text) is valid for island sizes bigger than 1,000 atoms. The elastic constants used for the strain relaxation are given in Tab. I. The surface energies stresses are those of Tab. 4. For the edge energy we used $\gamma^{\text{edge}} = 50$ meV/Å.

larger than ~ 16 atoms, so that the reconstructions on the facets are not suppressed and therefore the surface energy scales then with the area. This implies it scales with the volume to the power 2/3. Surface energy is a cost, and therefore the contribution is positive. Also shown is the contribution from the edges which also is a cost, though a rather small one. Obviously, the sum over the energies of the edges scales with the volume to the power 1/3. So that the edge energies provide the scaling relation they should be larger than ~ 4 atoms. The main uncertainty in using the above approach is that there are no edge energies known until now and they only can be estimated. Furthermore, for small islands the atomic structure on the side facets might not reconstruct.

This method of calculating the total energy of dislocation-free, strained, relaxed islands (as described by Eq. 1) was used before^{17,18} but so far some approximations were implied which will now be dropped. The approximations were: *i*) the elastic properties of the InAs islands were taken identical to those of the GaAs substrate, *ii*) the influence of the surface strain on the surface energies of the various facets was neglected, *iii*) the influence of the edge energies was not discussed. The improved treatment reported in this paper required elaborate calculations (this applies in particular to the surface

stresses), but our results fully confirm the earlier conclusions. The obtained quantitative differences to the previous work are small.

In the following Section we discuss some results of the finite element calculations. Then, Section III presents the calculations of surface energies and surfaces stresses for the low-index surfaces: (001), (110), (111), and ($\bar{1}\bar{1}\bar{1}$). For the (110) surface we also give the results for the first derivative of the surfaces stress with respect to strain. Combining the results for elastic and surface energies we obtain the total energy of the islands, and from the total energies of all different island shapes we derive the energetically favorable island shape for a given volume. This analysis is done in Section IV, where we also discuss the influence of the edge energies.

II. LONG-RANGE STRAIN RELAXATION IN THE ISLAND AND THE SUBSTRATE

We have calculated the elastic energy within the continuum theory. The experimental elastic moduli (see Tab. I) are used to describe the elastic properties of both the substrate and the island. A finite element approach is applied to solve the elasticity problem. Both the island and a sufficiently thick slab (240 Å for a quantum dot volume of 2.88×10^5 Å³) representing the substrate are divided into small irregularly shaped tetrahedra. The displacement field is tabulated on the vertices of this partitioning. Within each tetrahedron the linear interpolation of the displacement field is uniquely determined by the values at the four corners of the tetrahedron. The total elastic energy is calculated by summing the elastic energy density within each tetrahedron, which is a function of local strain, times the volume of the unstrained tetrahedron over all tetrahedra. This expression is iteratively minimized with respect to the displacement field. This procedure is repeated for finer and finer partitioning of the volume and the results are finally extrapolated to fineness equal to zero.

To obtain the elastic energy of truncated islands we use a simple analytic approximation to avoid repeating the full finite-element calculation. This analytic expression is based on the scaling law for the elastic energy and on the fact that the tops of the pyramidal islands are almost completely relaxed. The islands relaxes about 50 %, if the substrate is kept fixed. Additional 15 % are gained if both island and substrate are relaxed. In Fig. 2 the strain

material	c_{11} [GPa]	c_{12} [GPa]	c_{44} [GPa]
GaAs	119	53.8	59.4
InAs	83.3	45.3	39.6

TABLE I. The experimental elastic moduli c_{11} , c_{12} and c_{44} of GaAs and InAs.¹⁹

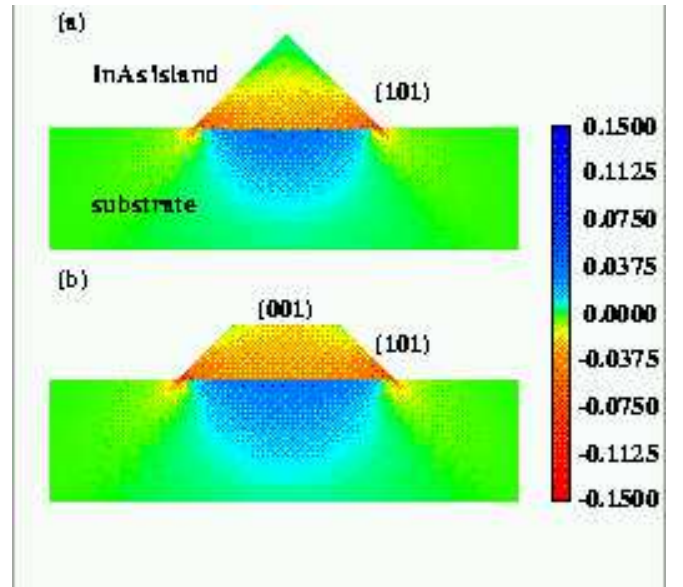


FIG. 2. The trace of the strain tensor for (a) a pyramidal and (b) a truncated island on the (010) cross sections through the islands. Note that the actual calculation has been carried out for a much thicker slab.

field of a pyramidal and a truncated island are compared. For both shapes the trace of the strain tensor is shown on a (010) cross section plane. The top of the pyramidal island is almost fully relaxed and therefore the elastic energy is almost completely stored in the base. From this observation and the scaling law of elastic energy with volume, one easily can derive the analytic approximation for the elastic relaxation energies of truncated pyramids which was proven to be sufficiently accurate.¹⁸

III. SURFACE ENERGIES, SURFACE STRESSES, AND THEIR FIRST DERIVATIVES

The InAs surface energies and surfaces stresses are calculated²⁰ using density-functional theory and the local-density approximation for the exchange-correlation energy functional.²¹ We use *ab initio*, norm-conserving, fully separable pseudopotentials.^{22–24} The wave functions are expanded into plane waves with an energy cutoff of 10 Ry. The \mathbf{k} -summation is done by using a uniform Monkhorst-Pack mesh²⁵ with a density equivalent to 64 \mathbf{k} -points in the whole (1 × 1) surface Brillouin zone of the (100) surface. To obtain the absolute surface energies for (111) and ($\bar{1}\bar{1}\bar{1}$) orientations we employ the energy-density formalism introduced by Chetty and Martin.²⁶ Corresponding calculations were done before for GaAs and are described in Ref. 27. As the InAs surface reconstructions are similar to those of GaAs,²⁸ we choose the same candidates for the low-energy surface structures. Indeed, we find the same behavior, except that

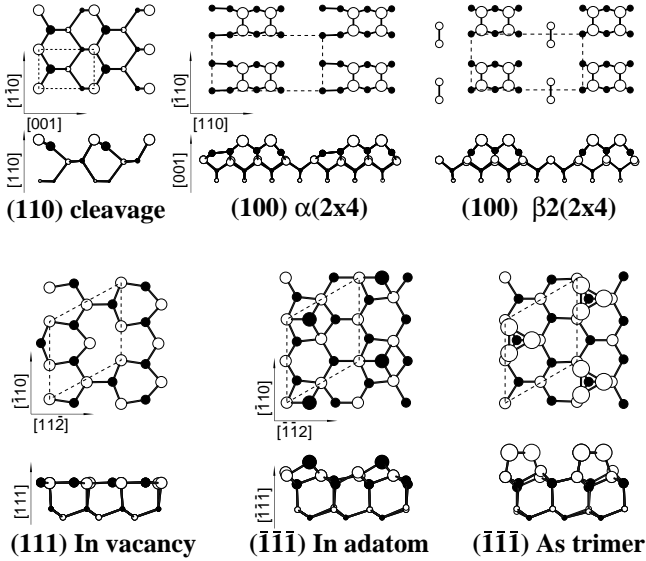


FIG. 3. Atomic structure models for the different InAs surfaces, top and side views. Filled and open circles denote In and As atoms, respectively.

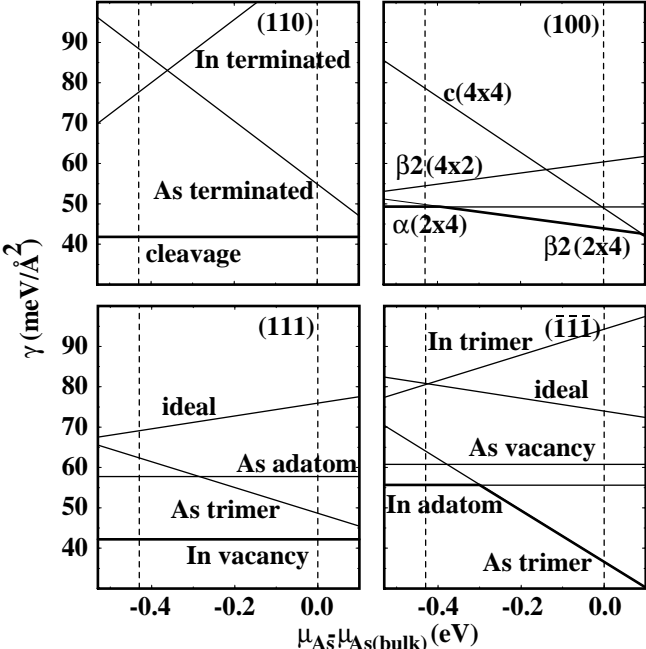


FIG. 4. InAs surface energies of the (110), (100), (111), and ($\bar{1}\bar{1}\bar{1}$) surface orientation as a function of the As chemical potential. The thick lines highlight the calculated surface energies of the reconstructions of lowest total energy.

As-rich reconstructions like the As terminated (110) surface are energetically unfavorable and not thermodynamically stable.

The relaxed atomic surface geometries of the equilibrium structures are displayed in Fig. 3. In Fig. 4 the surface energies are shown as function of the As chemical potential. The left and right vertical dashed lines denote a In and As-rich environment, respectively. For the

TABLE II. Surface energies γ and surface stresses σ_x , σ_y for InAs surface reconstructions in equilibrium with bulk As.

surface	γ (meV/Å ²)	σ_x (meV/Å ²)	σ_y (meV/Å ²)
(110) cleavage	41	26	54
(100) $\beta 2(2 \times 4)$	44	—	—
(111) In vacancy	42	48	48
(111) As trimer	36	92	92

(100) orientation the $\alpha(2 \times 4)$ and $\beta 2(2 \times 4)$ reconstructions have the lowest surface energy. Both the (110) and (111) surface energies are independent of the As chemical potential. The relaxed (1×1) cleavage surface is the stable reconstruction for the (110) orientation and the In vacancy structure for the (111) orientation. On the ($\bar{1}\bar{1}\bar{1}$) surface an As trimer reconstruction forms in As-rich environment. In In rich environment the In adatom structure is energetically preferred. We note that a $(\sqrt{19} \times \sqrt{19})$ structure had been observed in the case of GaAs by scanning tunneling microscopy.²⁹ However, we have not yet carried out calculations for this reconstruction, which would be rather expensive due to the large unit cell.

Because epitaxial growth is often performed under As-rich conditions, we present in Tab. II the surface energies for $\mu_{\text{As}} = \mu_{\text{As(bulk)}}$, *i.e.*, μ_{As} is taken at the value of the right dashed line of Fig. 4. Furthermore, we have calculated the surface stress for the reconstructions stable under As-rich conditions, and we calculated the strain derivatives of the stress. These results are required in order to obtain the corrections of the surface energy for strained systems. The surface energy of a strained surface defined with respect to the area of the undeformed surface is given by

$$\gamma^{\text{strained}} = \gamma + \sum_{ij} \sigma_{ij} \epsilon_{ij} + \frac{1}{2} \sum_{ijkl} \epsilon_{ij} S_{ijkl} \epsilon_{kl} + \dots, \quad (2)$$

where γ is the unstrained surface energy, σ_{ij} the surface stress tensor, ϵ_{ij} the strain tensor, and S_{ijkl} the tensor of second order stresses. The calculation of the first order surface stress is done as follows. We calculate the surface energy of a slab for various lattice constants in the range of $\pm 4\%$. The strained surfaces do not have to be relaxed again after straining because the relaxation energy is of second order in the strain. The energies of the strained surfaces are fitted to a polynomial from which we extract the linear coefficient of surface energy as a function of the strain. In all calculations we find that the components of the surface stress tensor are tensile. Compared to the Si (100) surface its value has the same order of magnitude.³⁰ For the (110) surface σ_x and σ_y denote components parallel to [001] and [110] respectively. For the (111) and ($\bar{1}\bar{1}\bar{1}$) surface the surface stress tensors are isotropic due to the three fold symmetry of the surface. For the (110) surface we also evaluated the strain derivative of the surface stress by compressing the surface isotropically up to 12 %. The surface energy of

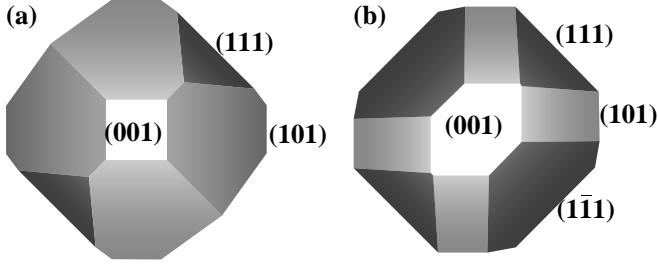


FIG. 5. The equilibrium crystal shape of InAs in (a) In-rich and (b) As-rich environment. The Miller indices of the surfaces are noted.

the strained surface is computed by subtracting the corresponding energy of strained bulk from the total energy of the relaxed strained slab. The surface energy as a function of the strain is fitted to a second order polynomial. The second order coefficient gives the sum of the derivatives of the surface stress $S_{1111} + 2S_{1122} + S_{2222}$ which is equal to $-0.5 \text{ eV}/\text{\AA}^2$. Straining the InAs (110) surface epitaxially to the GaAs lattice constant would result in a contribution from the second order terms to the surface energy smaller than $2 \text{ meV}/\text{\AA}^2$, while the linear term amounts to $\sim 6 \text{ meV}/\text{\AA}^2$. Thus we neglect in the following the second and higher order corrections to the surface energy.

Under thermal equilibrium conditions, the shape of a large InAs crystallite is given by the condition of lowest free energy. This can be obtained for zero temperature by applying the Wulff construction using the surface energies of Tab. II. The resulting shape is shown in Fig. 5. As this figure is constructed using only the surface energies of the {110}, {100}, {111}, and {1̄1̄1} orientations, we note that in general also higher index surfaces might be present, but the low Miller-index surfaces are expected to remain clearly prominent. Fig. 5 shows that under As-rich conditions all four considered surface orientations coexist on the equilibrium crystal shape. This result is in agreement with the shape of large, and thus presumably fully relaxed, InAs islands grown on a GaAs substrate by Steimetz *et al.*³¹ using metal-organic vapor-phase epitaxy. Under In-rich condition the {1̄1̄1} facets do not exist because they are energetically unfavorable. This is probably due to the fact that we did not consider the $(\sqrt{19} \times \sqrt{19})$ structure.

IV. EQUILIBRIUM SHAPE OF ISOLATED QUANTUM DOTS

The equilibrium shape of a strained coherent island of a given number of atoms is determined by the minimum of its total energy with respect to its shape. To determine the optimum island shape as a function of volume we follow the procedure already outlined in Ref. 18. As described in Section I the total energy is evaluated by

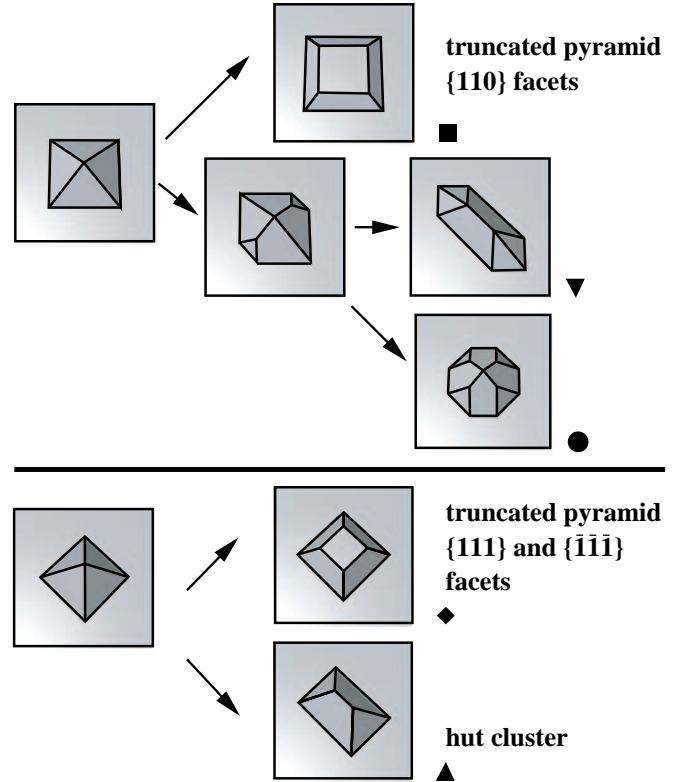


FIG. 6. The different island shapes which are investigated. They consist out of {101}, {001}, {111}, and {1̄1̄1} facets.

summing the elastic energy, the strain renormalized surface energy and the edge energy.

Accurate values of the edge energies are not known. We examined the influence of edge energies by calculating the equilibrium island shapes assuming the same value of the edge energy for all types of edges. We found that the island shape was not influenced as long as edge energies are smaller than $100 \text{ meV}/\text{\AA}$ for a quantum dot of 10,000 atoms, mainly because the edge energies only scale with $V^{1/3}$. Heller *et al.*³² measured the energies of steps on the GaAs (100) surface to be $4 \text{ meV}/\text{\AA}$ and $13 \text{ meV}/\text{\AA}$ for the two different types of steps. Recently, Kratzer and Scheffler³³ computed a value of $25 \text{ meV}/\text{\AA}$ for the one type. Edge energies should be of comparable size or even smaller and thus do not play a role for the island shape. Therefore, we neglect the edge energies in the following analysis.

Due to the different scaling properties of the elastic and surface energy, the optimum island shape depends on the volume. We consider all possible island shapes which have low-index surface facets. An overview is shown in Fig. 6. If surfaces with other orientations and a smaller slope than the {101} facets would appear on the islands, these surfaces would facet into the thermodynamically stable orientations {101}, {001}, {111}, and {1̄1̄1}. We calculate the total energies of islands bounded by {101}, {111}, and {1̄1̄1} facets. The filled symbols in Fig. 7 are

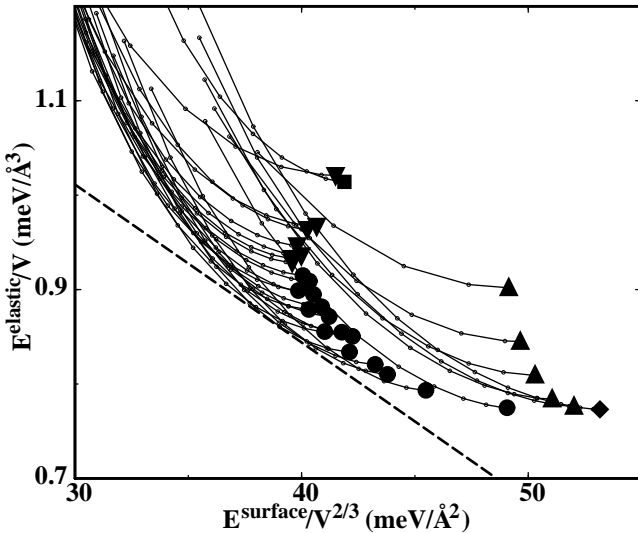


FIG. 7. The elastic energy per volume E^{elastic}/V versus the surface energy per area $E^{\text{surface}}/V^{2/3}$ for InAs islands. The symbols refer to the shapes displayed in Fig. 6: *Square*: square based pyramid with four $\{101\}$ facets. *Diamond*: square based pyramid with two $\{111\}$ and two $\{\bar{1}\bar{1}\bar{1}\}$ facets. *Triangles up*: huts with two $\{111\}$ and two $\{\bar{1}\bar{1}\bar{1}\}$ facets. *Triangles down*: square based $\{101\}$ pyramids with $\{\bar{1}\bar{1}\bar{1}\}$ truncated edges. *Dots*: islands with four $\{101\}$, two $\{111\}$, and two $\{\bar{1}\bar{1}\bar{1}\}$ facets. The open circles denote the corresponding truncated islands which are connected by the full lines. The dashed line is the curve of constant total energy $E^{\text{elastic}} + E^{\text{surface}}$ that selects the equilibrium shape for the volume $V = 2.14 \times 10^5 \text{ Å}^3$.

obtained using results from full finite element calculations, whereas the small dots denote the truncated mesa shaped islands where the elastic energies are derived from the simple analytical approximation. The results of the elastic calculations are combined with the *ab initio* surface energies. Because the side facets of the islands are strained we include the first order correction of the surface energy due to the strain. For this we use the *ab initio* stress tensors from Tab. II and combine it with the strain field at the surface from the finite element calculation. We have used the surface energy of the unstrained InAs (100) surface for the almost fully relaxed (100) top facets of the quantum dots, and the surface energy of an isotropically strained wetting layer for the area covered by the quantum dots. The contribution of the elastic and strain renormalized surface energies are displayed in Fig. 7, both of them divided by the their respective scaling factors.

In Fig. 7 the optimum island shape is determined by the point where the line of constant total energy touches the manifold of the island energies from below. Therefore, the equilibrium island shapes for all volumes are given by the lower envelope of the manifold of the island energies. In Fig. 8 the equilibrium island shapes determined by this method are shown for two different volumes. The elastic energy scales with the volume V

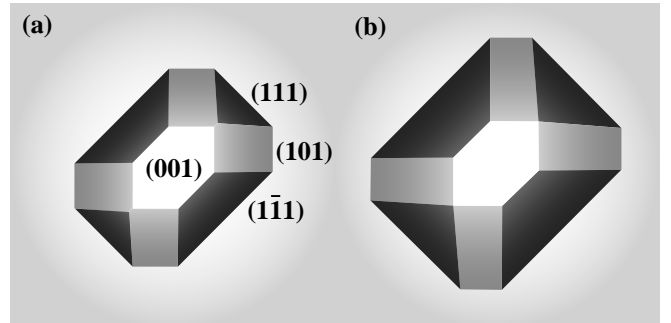


FIG. 8. The equilibrium shape of a strained coherent InAs islands in As rich environment at two different volumes, (a) $V \approx 2 \times 10^5 \text{ Å}^3$ (10,000 atoms), (b) $V \approx 4 \times 10^5 \text{ Å}^3$ (20,000 atoms).

whereas the strain renormalized surface energy increases with the volume like $V^{2/3}$, because the strain field of the side facets is invariant to the scaling. Due to their scaling the surface energy dominates at small volume and the elastic energy gains more importance at large volume. Thus, larger islands are steeper than smaller ones. As the $\{111\}$ and $\{\bar{1}\bar{1}\bar{1}\}$ facets are steeper than the $\{101\}$ facets they become more prominent on larger islands. Therefore, the island shape is not fixed, but changes continuously with the volume. This change in the shapes implies that the simple scaling laws which are valid for a fixed shape do not apply.

The influence of the surface stress is in such a way that surface energies of the $\{111\}$ and $\{\bar{1}\bar{1}\bar{1}\}$ facets are further lowered as compared to the $\{101\}$ facets. Roughly 30 % of the surface of each facets are strained while the rest is completely relaxed. This means that the $\{101\}$ facets are lowered due to the strain by $\Delta\gamma = -1.7 \text{ meV/Å}^2$ whereas the $\{111\}$ and $\{\bar{1}\bar{1}\bar{1}\}$ facets are lowered by $\Delta\gamma = -2.1 \text{ meV/Å}^2$ and $\Delta\gamma = -4.1 \text{ meV/Å}^2$, respectively, i.e., the $\{\bar{1}\bar{1}\bar{1}\}$ facets are lowered 6 % more in surface energy than the $\{101\}$ facets. Thus, the $\{\bar{1}\bar{1}\bar{1}\}$ faces dominate even more due to the surface strain. Although influenced by strain effects the equilibrium island shape remains similar to the ECS.

Recent atomic force microscopy (AFM) studies by Georgsson *et al.*⁶ of uncapped (not overgrown) InP islands on a GaInP substrate corroborate our theoretical predictions. The experimental island shape displays the same facets as our calculated island shape. Although InP differs from InAs, *ab initio* results³⁴ yield a similar behavior for the surface energies of InP as for InAs. Therefore, we expect to obtain a similar theoretical shape for InP islands. For InAs, however, the experimentally observed shapes differ from ours and show various different shapes. Moison *et al.*³ observe $\{410\}$ to $\{110\}$ facets and Ruvimov *et al.*⁴ only $\{110\}$ facets. Whereas Leonard *et al.*² report their island shapes as planoconvex lenses with a radius to height aspect ratio of about two. The great diversity of experimental island shapes and the difference to ours indicates that the respective growth conditions do

not represent thermodynamic equilibrium but are driven by kinetics. Thus, kinetic effects such as Jesson *et al.*¹⁰ suggested may play a role. These kinetic effects could not only affect the distribution of the island size but also the shape of the islands. However, it should be possible to achieve thermodynamic equilibrium by choosing appropriate experimental conditions. Alloying of the quantum dots with the GaAs matrix will also play a role and might affect the shape of the quantum dots.¹⁵

To gain further insight into the shape of the islands, more experimental investigations should be performed such as high resolution STM or AFM of the side facets. This could help the theory for further investigations.

V. ACKNOWLEDGMENTS

This work was supported in part by the Sfb 296 of the Deutsche Forschungsgemeinschaft.

* Electronic Address: moll@fhi-berlin.mpg.de

¹ S. Guha, A. Madhukar, and K. C. Rajkumar, *Appl. Phys. Lett.* **57**, 2110 (1990).

² D. Leonard, K. Pond, and P. M. Petroff, *Phys. Rev. B* **50**, 11687 (1994).

³ J. M. Moison, F. Houzay, F. Barthe, L. Leprince, E. Andreè, and . Vatet, *Appl. Phys. Lett.* **64**, 196 (1994).

⁴ S. Ruvimov, P. Werner, K. Scheerschmidt, U. Gösele, J. Heydenreich, U. Richter, N. N. Ledentsov, M. Grundmann, D. Bimberg, V. M. Ustinov, A. Y. Egorov, A. E. Zhukov, P. S. Kop'ev, and Z. I. Alferov, *Phys. Rev. B* **51**, 14766 (1995).

⁵ M. Grundmann, J. Christen, N. N. Ledentsov, J. Böhrer, D. Bimberg, S. S. Ruvimov, P. Werner, U. Richter, U. Gösele, J. Heydenreich, V. Ustinov, A. Egorov, A. Zhukov, P. Kop'ev, and Z. I. Alferov, *Phys. Rev. Lett.* **74**, 4043 (1995).

⁶ K. Georgsson, N. Carlsson, L. Samuelson, W. Seifert, and L. R. Wallenberg, *Appl. Phys. Lett.* **67**, 2981 (1995).

⁷ N. N. Ledentsov, M. Grundmann, N. Kirstaedter, O. Schmidt, R. Heitz, J. Böhrer, D. Bimberg, V. M. Ustinov, V. A. Shchukin, A. Y. Egorov, A. E. Zhukov, S. Zaitsev, P. S. Kop'ev, Z. I. Alferov, S. S. Ruvimov, A. O. Kosogov, P. Werner, U. Gösele, and J. Heydenreich, *Solid State Electron.* **40**, 785 (1996).

⁸ N. N. Ledentsov, in *Proceedings of the 23rd International Conference on the Physics of Semiconductors*, edited by M. Scheffler and R. Zimmermann (World Scientific, Singapore, 1996), p. 19.

⁹ I. N. Stranski and L. von Krastanow, *Sitzungsber. Akad. Wiss. Lit. Wien Math. Naturwiss. Kl. Abt. 2B Chemie* **146**, 797 (1937).

¹⁰ D. E. Jesson, K. M. Chen, and S. J. Pennycook, *MRS Bulletin* **21**, 31 (1996).

¹¹ Y. Chen and J. Washburn, *Phys. Rev. Lett.* **77**, 4046 (1996).

¹² H. T. Dobbs, D. D. Vvedensky, A. Zangwill, J. Johansson, N. Carlsson, and W. Seifert, *Phys. Rev. Lett.* **79**, 897 (1997).

¹³ V. A. Shchukin, N. N. Ledentsov, P. S. Kop'ev, and D. Bimberg, *Phys. Rev. Lett.* **75**, 2968 (1995).

¹⁴ V. A. Shchukin, N. N. Ledentsov, M. Grundmann, P. S. Kop'ev, and D. Bimberg, *Surf. Sci.* **352**, 117 (1996).

¹⁵ A. Rosenauer, U. Fischer, D. Gerthsen, and A. Förster, *Appl. Phys. Lett.* **71**, 3868 (1997).

¹⁶ C. Priester and M. Lannoo, *Phys. Rev. Lett.* **75**, 93 (1995).

¹⁷ E. Pehlke, N. Moll, and M. Scheffler, in *Proceedings of the 23rd International Conference on the Physics of Semiconductors*, edited by M. Scheffler and R. Zimmermann (World Scientific, Singapore, 1996), p. 1301.

¹⁸ E. Pehlke, N. Moll, A. Kley, and M. Scheffler, *Appl. Phys. A* **65**, 525 (1997).

¹⁹ *Landolt-Börnstein*, edited by K.-H. Hellwege (Springer-Verlag, Berlin, 1982), Vol. III.

²⁰ M. Bockstedte, A. Kley, J. Neugebauer, and M. Scheffler, *Comput. Phys. Commun.* **107**, 187 (1997).

²¹ J. P. Perdew and A. Zunger, *Phys. Rev. B* **23**, 5048 (1981).

²² D. R. Hamann, *Phys. Rev. B* **40**, 2980 (1989).

²³ M. Fuchs and M. Scheffler, <http://www.fhi-berlin.mpg.de/th/fhi96md/code.html> (unpublished).

²⁴ L. Kleinman and D. M. Bylander, *Phys. Rev. Lett.* **48**, 1425 (1982).

²⁵ H. J. Monkhorst and J. D. Pack, *Phys. Rev. B* **13**, 5188 (1976).

²⁶ N. Chetty and R. M. Martin, *Phys. Rev. B* **45**, 6089 (1992).

²⁷ N. Moll, A. Kley, E. Pehlke, and M. Scheffler, *Phys. Rev. B* **54**, 8844 (1996).

²⁸ P. N. Fawcett, in *Properties of Lattice-Matched and Strained Indium Gallium Arsenide*, edited by P. Bhattacharya (INSPEC, the Institution of Electrical Engineers, London, United Kingdom, 1993), p. 133.

²⁹ D. K. Biegelsen, R. D. Bringans, J. E. Northrup, and L.-E. Swartz, *Phys. Rev. Lett.* **65**, 452 (1990).

³⁰ A. García and J. E. Northrup, *Phys. Rev. B* **48**, 17350 (1993).

³¹ E. Steimetz, F. Schienle, and W. Richter, *J. Cryst. Growth* **170**, 208 (1997).

³² E. J. Heller, Z. Y. Zhang, and M. G. Lagally, *Phys. Rev. Lett.* **71**, 743 (1993).

³³ P. Kratzer and M. Scheffler (unpublished).

³⁴ N. Moll and M. Scheffler (unpublished).